

Jammed Keplerian gas leads to the formation and disappearance of spiral arms in a coupled map lattice for astronomical objects

Erika Nozawa¹

Department of Physics, Faculty of Core Research, Ochanomizu University,
2-1-1 Ohtsuka, Bunkyo-ku, Tokyo 112-8610, Japan

Abstract

The formation and disappearance of spiral arms are studied by focusing on jammed Keplerian gas in a coupled map lattice (CML) with a minimal set of procedures for simulating diverse patterns in astronomical objects. The CML shows that a spiral arm is a type of traffic jam, and its motion is governed by both a gas inflow into and outflow from the jam. In particular, a new mechanism for the disappearance of spiral arms is found. It is caused not by conventional differential rotation, but by the gas flow rate difference between the light inflow and heavy outflow, here called "light-in and heavy-out", leading to the disappearance of traffic jams. Furthermore, we propose a general approximate formula for the lifetime of spiral arms, which is simply derived from the mechanism of the "light-in and heavy-out". The proposed formula is successfully applied to the CML simulations, and moreover, to the observational data of the spiral galaxy M51.

1. Introduction

Coupled map lattice (CML) is a useful dynamical system with discrete space and time, and continuous state variables [1, 2]. It well reproduces experimental observations in spatially extended dynamical phenomena [3–6], and is quite useful to find essential elementary processes in such phenomena [1–6]. Furthermore, fast computation of CML may give us insightful suggestions on undiscovered phenomena or unsolved problems. Indeed, we have proposed a CML for astronomical objects to study the spiral pattern formation of accreting cold dense gas, such as seen in spiral galaxies [7] or protoplanetary disks [8], and simulated dynamic patterns and properties agreeing with the several results of the conventional theories [7, 9] and observations [10–13], as reported in the previous paper [14]. Moreover, we suggest that the CML should give an answer to unsettled questions about the formation mechanism of spiral arms, especially the disappearance of spiral arms, which is presented in this paper.

In astrophysics, the formation mechanism of spiral arms has attracted much attention and has been studied with various models [7]. However, the mechanism has not been fully understood yet. There still remains important unsettled issues such as whether spiral arms are stationary or transient [7, 15], and what the origin of spiral arms is [7, 16]. For example, as a well-known question, it has been discussed if spiral arms are density waves [9, 17] or material arms [18, 19], since about sixty years ago to this day. Recently, some observations support the density wave theory [13].

In this paper, we argue that spiral arms are a type of traffic jam formed by jammed Keplerian gas around a central star, and therefore transient in terms of the disappearance of traffic jams [20], based on the CML simulations.

The disappearance of spiral arms has been discussed as the "winding up of spiral arms" caused by differential rotation in not only material arms [7], but also density waves [15]. However, the CML presents a new disappearance mechanism of spiral arms caused by the gas flow rate difference between a light inflow into and heavy outflow from the jam, which we call "light-in and heavy-out". This gas flow rate difference decreases the mass of traffic jams, and leads to the disappearance of them, and therefore in that sense spiral arms are transient. The "light-in and heavy-out" is consistent with the well known fact in astrophysics that gas clumps flow into spiral arms, are compressed, and then flow out as massive gas clumps like stars [7] or possibly black holes [21]. Indeed, we find a gas flow rate difference which should correspond to the "light-in and heavy-out" in the observational data of the spiral galaxy M51 [13].

We propose a general approximate formula for the lifetime of spiral arms from the mechanism of the "light-in and heavy-out". It is simply given by dividing the mass of traffic jams by the gas flow rate difference between the inflow and outflow. The approximate values obtained agree with the lifetimes in the CML simulations well. Furthermore, we apply the proposed formula to the observational data of the spiral galaxy M51 [13], and obtain the approximate value in agreement with the conventional theories [22] within the expected range.

The present paper is organized as follows. In Section 2, we explain briefly a CML for astronomical objects, which we have introduced in [14]. In Section 3, we study the dynamic properties of a spiral arm from three aspects as traffic jams. First, the formation of the spiral arm occurs due to the jammed motion of Keplerian gas passing through the arm. Second, the motion of the spiral arm is given as the movement of the traffic jam. Third, the disappearance of the spiral arm and especially its characterizing lifetime are caused by the gas flow rate difference

¹E-mail address: papers@e-rika.net

between the light inflow into and heavy outflow from the arm, which is called the "light-in and heavy-out". In Section 4, we compare the above results with the observations in a spiral galaxy. Summary and discussion are given in Section 5.

2. Model

We briefly review a coupled map lattice (CML) for simulating diverse patterns, especially spiral patterns, in astronomical objects [14]. The CML consists of a minimal set of procedures: gravitational interaction and advection.

We study a system of accreting cold dense gas moving on a two-dimensional region, such as an accretion disk well known in active galactic nuclei and protoplanetary disks [7]. The region is divided into $N_x \times N_y$ square cells. The gas in each cell forms a macroscopic gas clump through the collision of dense gas [7], which is treated as an assembly of virtual gas particles (not gas molecules). For simplicity, we assume that gas particles in each cell are distributed uniformly and carried by the same flow.

We introduce a finite two-dimensional square lattice by placing a lattice point on the center of each cell. The distance between the nearest neighbor lattice points is set to one, and each cell size is also one. The lattice points are labeled ij ($i = 0, 1, \dots, N_x - 1$ and $j = 0, 1, \dots, N_y - 1$) and their positions are given by the position vectors $\mathbf{r}_{ij} = (i, j) = i\mathbf{e}_x + j\mathbf{e}_y$, where \mathbf{e}_x and \mathbf{e}_y are unit vectors parallel to the x - and y -axis respectively.

We define two kinds of field variables, the mass m_{ij}^t and the velocity $\mathbf{v}_{ij}^t = v_{xij}^t \mathbf{e}_x + v_{yij}^t \mathbf{e}_y$ of the gas clump at lattice point ij at discrete time t . They are coarse-grained variables given by the total mass and the flow of gas particles in the cell at lattice point ij , respectively.

We decompose the spiral pattern formation in astronomical objects into two important elementary processes, a gravitational interaction process and an advection process. In the former process, the gas clump velocity \mathbf{v}_{ij}^t is changed by the gravitational interaction among gas clumps. In the latter process, the gas clump mass m_{ij}^t and velocity \mathbf{v}_{ij}^t are changed since gas particles move and collide to form new gas clumps by the flows, i.e., the gas clump velocities resulting from the former process.

We formulate the gravitational interaction process as an Eulerian procedure [1, 4] T_g in the lattice picture [14]. In the procedure T_g , the gas clump velocity \mathbf{v}_{ij}^t is changed to \mathbf{v}_{ij}^* due to the gravitational interaction from the other gas clumps at lattice points kl , where $*$ represents an intermediate time between discrete times t and $t + 1$. The procedure T_g is defined by the following maps:

$$m_{ij}^* = m_{ij}^t, \quad (1)$$

$$\mathbf{v}_{ij}^* = \mathbf{v}_{ij}^t - \gamma \tau_g \sum_{k=0}^{N_x-1} \sum_{l=0}^{N_y-1} \frac{(1 - \delta_{ik} \delta_{jl}) m_{kl}^t}{|\mathbf{r}_{ij} - \mathbf{r}_{kl}|^2} \frac{\mathbf{r}_{ij} - \mathbf{r}_{kl}}{|\mathbf{r}_{ij} - \mathbf{r}_{kl}|}, \quad (2)$$

where γ is the gravitational constant, τ_g the time interval for the procedure T_g and δ the Kronecker delta. As shown in Eq. 1, the gas clump mass m_{ij}^t does not change in the procedure T_g .

We formulate the advection process as a Lagrangian procedure [1, 4] T_a in the particle picture [14]. In the procedure T_a , each flow \mathbf{v}_{kl}^* resulting from the procedure T_g carries gas particles with their total mass m_{kl}^* and momentum $m_{kl}^* \mathbf{v}_{kl}^*$ from the cell at lattice point kl to a cell-sized area centered at the position

$$(\tilde{k}, \tilde{l}) = (k + v_{xkl}^* \tau_a, l + v_{ykl}^* \tau_a), \quad (3)$$

where τ_a is the time interval for the procedure T_a . When the cell-sized areas overlap the cell at lattice point ij , the size w_{ijkl}^* of each overlap area is given by [14]

$$w_{ijkl}^* = \left(\delta_{i[\tilde{k}]} \delta_{j[\tilde{l}]} + \delta_{i[\tilde{k}]+1} \delta_{j[\tilde{l}]} + \delta_{i[\tilde{k}]+1} \delta_{j[\tilde{l}]+1} + \delta_{i[\tilde{k}]} \delta_{j[\tilde{l}]+1} \right) \left(1 - |\tilde{k} - i| \right) \left(1 - |\tilde{l} - j| \right), \quad (4)$$

where $[\bullet]$ is the floor function. In the cell at lattice point ij , gas particles in the overlap areas collide with each other and are mixed into one clump. This collision and mixture lead to the formation of a new gas clump whose mass and velocity are m_{ij}^{t+1} and \mathbf{v}_{ij}^{t+1} respectively. Thus, the advection procedure T_a is defined by the following maps:

$$m_{ij}^{t+1} = \sum_{k=0}^{N_x-1} \sum_{l=0}^{N_y-1} w_{ijkl}^* m_{kl}^*, \quad (5)$$

$$\mathbf{v}_{ij}^{t+1} = \frac{1}{m_{ij}^{t+1}} \sum_{k=0}^{N_x-1} \sum_{l=0}^{N_y-1} w_{ijkl}^* m_{kl}^* \mathbf{v}_{kl}^*. \quad (6)$$

In Eq. 6, when gas clump mass m_{ij}^{t+1} vanishes, gas clump velocity \mathbf{v}_{ij}^{t+1} is set to be also zero. We may operate the procedure T_a of Eqs. 5 and 6 with a low computational cost of $O(N)$, where N is the total number of lattice points [14].

We construct the time evolution of gas clump mass m_{ij}^t and velocity \mathbf{v}_{ij}^t for one step (from discrete time t to $t + 1$) by the following successive operations of the gravitational interaction procedure T_g and the advection procedure T_a :

$$\begin{pmatrix} m_{ij}^t \\ \mathbf{v}_{ij}^t \end{pmatrix} \xrightarrow{T_g} \begin{pmatrix} m_{ij}^* \\ \mathbf{v}_{ij}^* \end{pmatrix} \xrightarrow{T_a} \begin{pmatrix} m_{ij}^{t+1} \\ \mathbf{v}_{ij}^{t+1} \end{pmatrix}. \quad (7)$$

On the time evolution of Eq. 7, the total mass $\sum_{i,j} m_{ij}^t$, total momentum $\sum_{i,j} m_{ij}^t \mathbf{v}_{ij}^t$ and total angular momentum $\sum_{i,j} \mathbf{r}_{ij} \times m_{ij}^t \mathbf{v}_{ij}^t$ of the system are conserved [14].

The simulations are performed according to the following settings: Lattice size $N_x \times N_y$ is 50×50 ; Gravitational constant γ is one and time intervals τ_g and τ_a one; The initial gas clump mass m_{ij}^0 is given by a uniform random number within $[0, 2/(N_x N_y)]$; The initial gas clump velocity \mathbf{v}_{ij}^0 is given by zero; The boundary conditions are open. In the simulations, the total mass, total momentum and total angular momentum are not conserved completely, since gas particles move out through the boundary

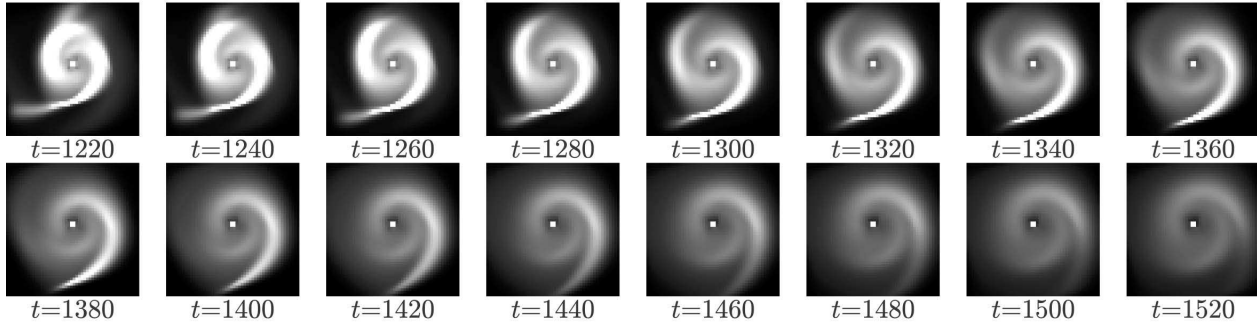


Figure 1: Snapshots of gas clump masses m_{ij}^t . The brightness of cells represents the gas clump mass m_{ij}^t ($i = 0, 1, \dots, 49$, $j = 0, 1, \dots, 49$ and $t = 1220, 1240, \dots, 1520$) in the range of 0 to 1.2×10^{-6} .

of the finite lattice. We note that the mass lost is a very small quantity (0.7% of the initial total mass) through the simulation shown in Fig. 1.

3. Dynamic properties of a spiral arm based on traffic jams

The formation and disappearance of spiral arms are simulated by the CML for astronomical objects. The results are shown as the snapshots in Fig. 1. The upper row snapshots (at $t = 1220, 1240, \dots, 1360$) roughly show the formation of spiral arms, and the lower row (at $t = 1380, 1400, \dots, 1520$) their disappearance. Each snapshot has 50×50 cells, and the brightness of the cells represents the gas clump mass m_{ij}^t . In the simulation, gas particles ejected from a contracting central star induce the traffic jams of Keplerian gas particles around the central star [14]. The jammed Keplerian gas particles form a pair of spiral arms and thus a grand design spiral pattern (that is, two-arm spiral pattern) appears, as in the snapshots at $t = 1220, 1240, \dots$, and 1360. After that, the spiral pattern disappears gradually with the disappearance of traffic jams, as in the snapshots at $t = 1380, 1400, \dots$, and 1520. Hereafter we focus on the time around $t = 1360$, the turning point from the formation to disappearance of spiral arms.

3.1. Motion of gas particles crossing a spiral arm

Gas particles move along Keplerian flows around the central star, and these Keplerian gas particles become jammed while crossing a spiral arm. The red dotted line in Fig. 2a shows a Keplerian flow which crosses the spiral arm from the left to the right at $t = 1360$. Figs. 2b and 2c show the density and speed changes of gas particles along the Keplerian flow, respectively. The results in Figs. 2b and 2c are obtained through the following three steps.

First, we define the Keplerian flow approximated as a circular flow at radial distance R from the center of gravity \mathbf{r}_S of the central star. As shown in Fig. 2a, the distance R is determined with the Keplerian flow crossing the most dense part of the spiral arm, which is located at the lattice points 24 6 and 25 6. Here the central star is located at

the lattice points 24 26, 25 26, 24 27 and 25 27, and the center of gravity \mathbf{r}_S is thus given by

$$\mathbf{r}_S = (x_S, y_S) = \frac{\sum_{i=24}^{25} \sum_{j=26}^{27} m_{ij}^t \mathbf{r}_{ij}}{\sum_{i=24}^{25} \sum_{j=26}^{27} m_{ij}^t}, \quad (8)$$

and the distance R is given by

$$R = y_S - 6. \quad (9)$$

Second, we rearrange cells (the red squares in Fig. 2a) along the Keplerian flow. The position vectors \mathbf{r}_i of rearranged cells i ($i = 15, 16, \dots, 34$) are given by

$$\mathbf{r}_i = (i, y_S + R \sin \theta(i)), \quad (10)$$

where $\theta(i)$ is an angle in the polar coordinate with pole \mathbf{r}_S and defined by

$$\theta(i) = \cos^{-1} \left(\frac{i - x_S}{R} \right) \quad (\pi \leq \theta(i) \leq 2\pi). \quad (11)$$

Third, using area-weighted average (see Appendix A), we obtain the average gas density $\tilde{m}_i = \tilde{m}^t(\mathbf{r}_i)/1$, velocity $\tilde{\mathbf{v}}_i = \tilde{\mathbf{v}}^t(\mathbf{r}_i)$ (the orange arrows in Fig. 2a), and speed $|\tilde{\mathbf{v}}_i|$ in rearranged cell i . Figs. 2b and 2c show the average gas density \tilde{m}_i and speed $|\tilde{\mathbf{v}}_i|$ respectively.

Fig. 2 clearly shows the jammed motion of Keplerian gas particles in the arm. While crossing the arm, Keplerian gas particles change their motion as follows: (1) When they flow into the arm ($i = 20, \dots, 24$ in Fig. 2a), density \tilde{m}_i increases rapidly (from 3.4×10^{-7} to 1.9×10^{-6} in Fig. 2b) and thus speed $|\tilde{\mathbf{v}}_i|$ is decelerated quickly (from 0.24 to 0.21 in Fig. 2c); (2) In the arm ($i = 24, \dots, 27$ in Fig. 2a), they are jammed, that is, keep high density \tilde{m}_i (in the range of 1.4×10^{-6} to 2.0×10^{-6} in Fig. 2b) and move with lower speed $|\tilde{\mathbf{v}}_i|$ (0.21 in Fig. 2c); (3) When they flow out of the arm ($i = 27, \dots, 34$ in Fig. 2a), density \tilde{m}_i decreases slowly (from 1.4×10^{-6} to 5.5×10^{-7} in Fig. 2b) and thus speed $|\tilde{\mathbf{v}}_i|$ is accelerated gradually (from 0.21 to 0.22 in Fig. 2c).

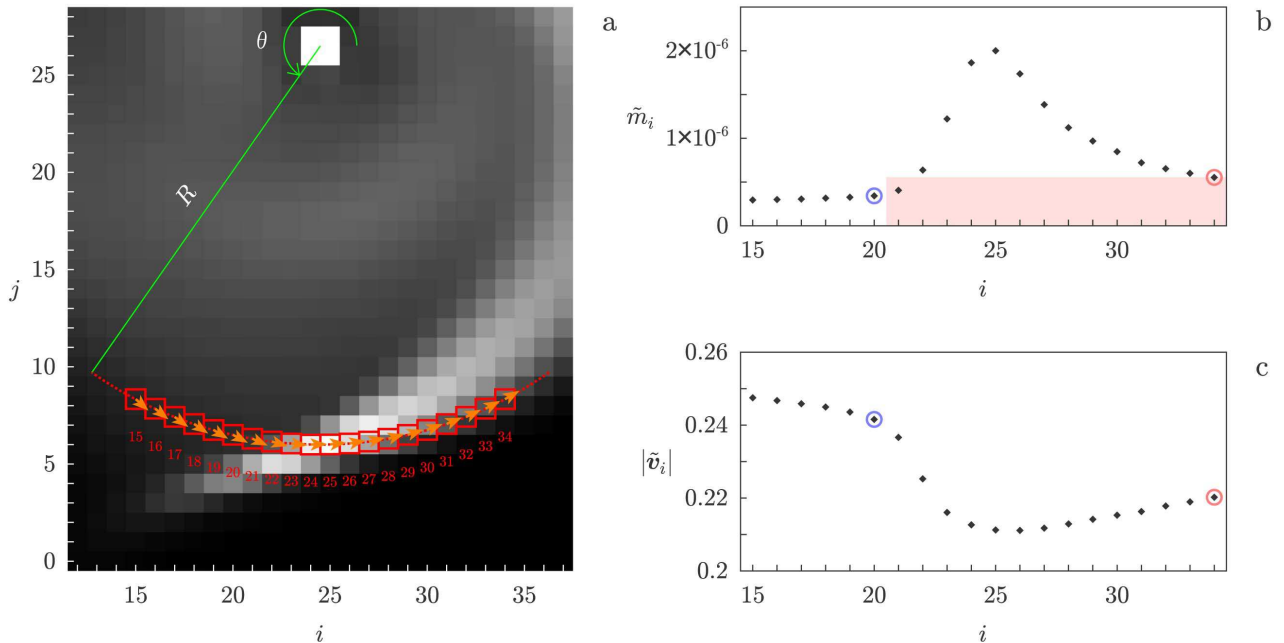


Figure 2: Motion of gas particles crossing the arm along the circular flow around the central star. (a) Circular flow around the central star. The brightness of cells represents gas clump masses m_{ij}^t in the range of 0 to 2×10^{-6} , the red dotted line the circular flow, the red squares rearranged cells i ($i = 15, 16, \dots, 34$) and the orange arrows average gas clump velocities \tilde{v}_i . (b) Average gas clump density \tilde{m}_i . (c) Average gas clump speed $|\tilde{v}_i|$.

The jammed motion of gas particles also occurs in other Keplerian flows at different radial distance R and different time t . Furthermore, the results in Fig. 2 are qualitatively in good agreement with the observations in the spiral galaxy M51 [13], as discussed in Section 4.

3.2. Motion of a spiral arm

A spiral arm is a type of traffic jam formed by high dense jammed Keplerian gas particles, as described in the previous subsection. This traffic jam moves along the circular flow not only with the velocity v_g of jammed Keplerian gas particles, but also with the velocity v_{io} caused by both a gas inflow into and outflow from the jam. This circular movement of the traffic jam is observed as the rotation of the spiral arm with the velocity

$$v_j = v_g + v_{io}. \quad (12)$$

The velocity v_{io} is opposite to the velocity v_g , which is well known as a property of traffic jams. We briefly explain the opposite velocity v_{io} . In the tail of the traffic jam (cells $i \leq 23$ in Fig. 2), Keplerian gas particles are decelerated to be part of the jam, and thus the tail of the jam becomes longer. On the other hand, in the front of the jam (cells $i \geq 27$ in Fig. 2), jammed Keplerian gas particles are accelerated to leave the jam, and thus the front of the jam becomes shorter. The longer tail and shorter front leads to the backward movement of the jam with the opposite velocity v_{io} ($v_{io} < 0$). Therefore, the traffic jam moves with the velocity v_j less than the velocity v_g of jammed Keplerian gas particles.

We obtain the three velocities v_j , v_g and v_{io} to verify their relationship described above. First, the velocity v_j of the arm is calculated as follows. Figs. 3a and 3b show the snapshots of gas clump masses m_{ij}^t at $t = 1350$ and 1360 respectively. In Fig. 3, the arm is in counterclockwise rotation. The rotation angle $\Delta\theta$ is given by about $\pi/60$ for a short period of time $\Delta t = 10$ steps and the radial distance R by around 20. Thus, the velocity v_j is given by

$$v_j = \frac{\Delta\theta}{\Delta t} R \sim \frac{\pi/60}{10} \times 20 \sim 0.1. \quad (13)$$

Second, the velocity v_g of jammed Keplerian gas particles becomes $v_g \sim 0.2$ as already shown in Fig. 2c. Third, from Eq. 12, the velocity v_{io} is given by

$$v_{io} = v_j - v_g \sim -0.1. \quad (14)$$

Thus, it is verified that the velocity v_{io} is opposite to the velocity v_g of jammed Keplerian gas particles, and the velocity v_g of the arm is slower than the velocity v_g .

In the previous and present subsections, the dynamic properties of the spiral arm have been studied. They agree with those of density waves [9] well, except that the spiral arm is transient, as discussed in the following subsection.

3.3. Disappearance of a spiral arm

We now argue that the "light-in and heavy-out" should underlie the disappearance of spiral arms, and therefore spiral arms are transient. In addition, we propose a general approximate formula for the lifetime of spiral arms, which is simply derived from the "light-in and heavy-out".

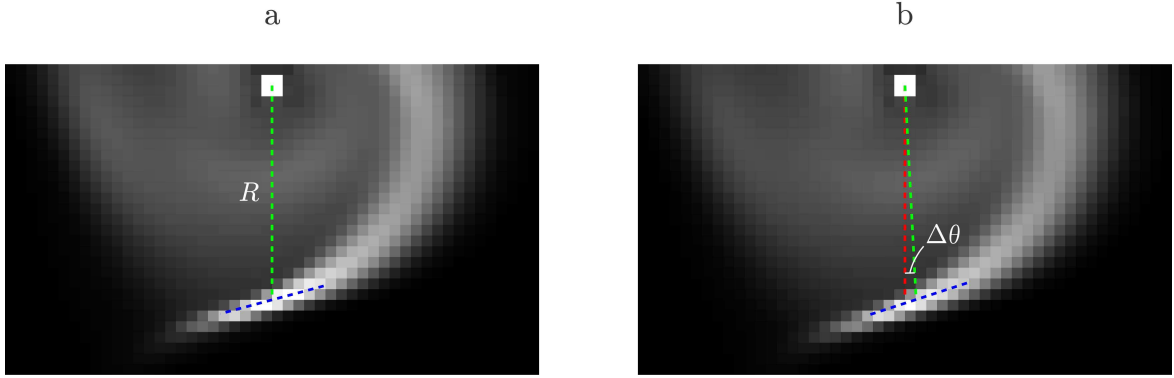


Figure 3: Rotation of the spiral arm. (a) Snapshot of gas clump masses m_{ij}^t at $t = 1350$. (b) Same, but for $t = 1360$. The green dotted lines are drawn from r_S to the center of the blue dotted lines parallel to the arm. The green dotted line at $t = 1360$ is rotated by $\Delta\theta$ from the red dotted line.

The "light-in and heavy-out" is the gas flow rate difference between the light inflow into and heavy outflow from a traffic jam in spiral arms. Here the gas inflow rate (and also outflow rate) is given by the product of its density and speed.

In Fig. 2b, the outflow gas density $m_{out} = \tilde{m}_{34}$ (the red circle in Fig. 2b) at the front of the traffic jam is about two times higher than the inflow gas density $m_{in} = \tilde{m}_{20}$ (the blue circle in Fig. 2b) at the tail. This is because gas particles are jammed and compressed, so that they become massive gas clumps in the jam, which we interpret as the formation of stars [7] or possibly black holes [21].

In Fig. 2c, the outflow gas speed $v_{out} = |\tilde{v}_{34}|$ (the red circle in Fig. 2c) at the jam front is slower than the inflow gas speed $v_{in} = |\tilde{v}_{20}|$ (the blue circle in Fig. 2c) at the jam tail, but the ratio v_{out}/v_{in} is almost one. This is because gas particles are in Keplerian motion.

As a consequence of the above discussion, the gas outflow rate $m_{out}v_{out}$ at the jam front is more than the gas inflow rate $m_{in}v_{in}$ at the jam tail. This gas flow rate difference $m_{out}v_{out} - m_{in}v_{in}$ decreases the mass m_{jam} of the jam, and leads to the disappearance of the traffic jam. Here we call this astronomical gas flow rate difference the "light-in and heavy-out".

Assuming that the gas flow rate difference $m_{out}v_{out} - m_{in}v_{in}$ is constant, the lifetime t_d of the spiral arm is simply given by the following general approximate formula:

$$t_d = \frac{m_{jam} - m_{ofs}}{m_{out}v_{out} - m_{in}v_{in}}. \quad (15)$$

The mass m_{jam} ($m_{jam} = \sum_{i=21}^{34} \tilde{m}_i \times 1$ in Fig. 2b) decreases gradually by the gas flow rate difference $m_{out}v_{out} - m_{in}v_{in}$. It reaches the mass m_{ofs} with the density m_{out} ($m_{ofs} = \sum_{i=21}^{34} m_{out} \times 1$ with the red rectangle in Fig. 2b), and finally the spiral arm disappears.

In order to verify the approximate formula Eq. 15, we calculate the lifetime of the spiral arm at $t = 1360$ shown in Fig. 2. The lifetime t_d is given by

$$t_d = \frac{1.5 \times 10^{-5} - 0.8 \times 10^{-5}}{1.2 \times 10^{-7} - 0.8 \times 10^{-7}} = 175. \quad (16)$$

Eq. 16 indicates that the spiral arm disappears at about $t = 1360 + t_d = 1535$, which is indeed confirmed with the spiral arm almost disappearing in the snapshot at $t = 1520$ in Fig. 1. In Eq. 15, we may use the average gas speed at radial distance R (for example, the Keplerian speed $\propto \sqrt{1/R}$) instead of the gas speeds v_{in} and v_{out} . This modification would be useful in observations, since gas velocity (or speed) is difficult to measure [13].

4. Comparison with observations

The dynamic properties of spiral arms in the CML simulations are qualitatively in good agreement with those in the gas (CO and H) observations of the spiral galaxy M51 [13]. According to [13], hereafter we divide the gas velocity into two components parallel and perpendicular to spiral arms in order to clearly show the velocity change including the gravity effect of spiral arms [7].

Figs. 4a1-4c1 show the observational data of gas crossing one of the paired spiral arms in M51 [13]. In each figure, the horizontal axis represents the spiral phase Ψ [deg] (i.e., the azimuthal angle from the spiral arm), and the vertical axis represents the surface density σ [M_\odot/pc^2] of gas, the parallel component V_{\parallel} [km/s] and perpendicular component V_{\perp} [km/s] of gas velocity, respectively. Figs. 4a2-4c2 show the modified results of Fig. 2 in order to make them correspond to Figs. 4a1-4c1 respectively. In each figure, the horizontal axis represents the index i of the rearranged cells in Eqs. 10 and 11, and the vertical axis represents the average gas density \tilde{m}_i , the parallel component $\tilde{v}_{i\parallel}$ and perpendicular component $\tilde{v}_{i\perp}$ of the average gas velocity \tilde{v}_i , respectively. The index i may be represented as the spiral phase $\Psi(i)$ given by

$$\Psi(i) = 2\theta(i) \sim 2 \left\{ \frac{180^\circ}{\pi R} (i - x_S) + 270^\circ \right\}, \quad (17)$$

with x_S , R and $\theta(i)$ given by Eqs. 8, 9 and 11 respectively.

The density and velocity changes in the observations and those in the CML simulations are similar, as shown

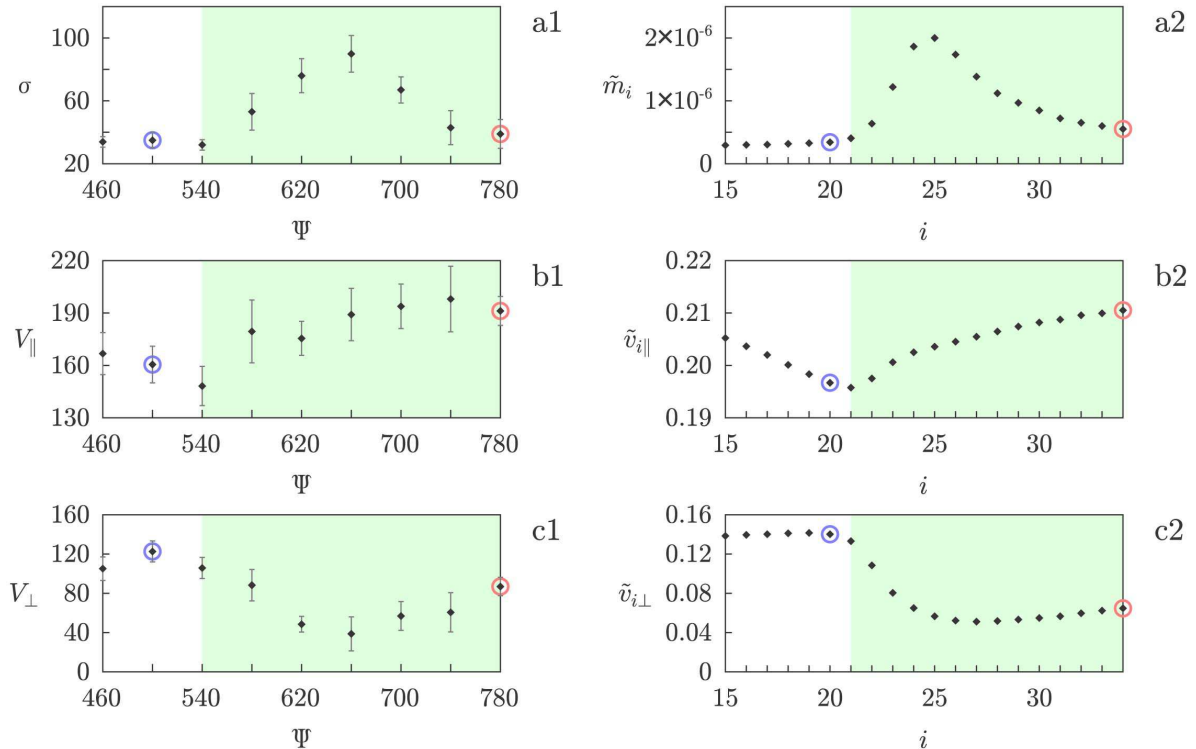


Figure 4: Observational data (a1), (b1), (c1) and CML simulation results (a2), (b2), (c2). (a1) Surface density σ [M_{\odot}/pc^2] of gas, (b1) Parallel component V_{\parallel} [km/s] and (c1) Perpendicular component V_{\perp} [km/s] of gas velocity. The horizontal axes represent the spiral phase Ψ [deg], and the gray bars the error bars. (a2) Average gas density \tilde{m}_i , (b2) Parallel component $\tilde{v}_{i\parallel}$ and (c2) Perpendicular component $\tilde{v}_{i\perp}$ of the average gas velocity \tilde{v}_i . In each figure, the green area represents the area of spiral arms.

in Figs. 4a1 and 4a2, Figs. 4b1 and 4b2, and Figs. 4c1 and 4c2 respectively. In the spiral arm ($\Psi = 540, 580, \dots, 780$ and $i = 21, 22, \dots, 34$ with the green areas in Fig. 4), the density σ and \tilde{m}_i increase greatly about 3- and 5-fold respectively. The parallel components V_{\parallel} and $\tilde{v}_{i\parallel}$ increase slightly about 1-fold (i.e., almost constant), and the perpendicular components V_{\perp} and $\tilde{v}_{i\perp}$ decrease significantly about 3-fold.

The good agreement between the changes in the simulations and the observations suggests that the traffic jam of gas should occur also in the actual spiral arm. The suggestion is consistent with the observational conclusion that the spiral arms of M51 are density waves [13], in that the dynamic properties of traffic jams and density waves are quite similar as described in Sections 3.1 and 3.2.

Moreover, we confirm a gas flow rate difference which should correspond to the "light-in and heavy-out" in the spiral arm of M51, by comparing Figs. 4a1-4c1 and Figs. 4a2-4c2. This suggests that the actual spiral arm also should be transient and have a lifetime. Here we take the gas flow rate $\sigma V = \sigma(V_{\parallel}^2 + V_{\perp}^2)^{1/2}$ at $\Psi = 500$ as the "light-in" (the blue circles in Figs. 4a1-4c1), and at $\Psi = 780$ as the "heavy-out" (the red circles in Figs. 4a1-4c1). By the general approximate formula Eq. 15, the life time t_d of the spiral arm of M51 is estimated as

$$t_d = \frac{m_{jam} - m_{ofs}}{m_{out}v_{out} - m_{in}v_{in}} \sim 150 \text{ [Myr]}, \quad (18)$$

with

$$\begin{aligned} m_{jam} &= \sum_{\Psi=540}^{780} \sigma(\Psi) [M_{\odot}/\text{pc}^2] \times 1100 [\text{pc}^2] \\ &= 4.4 \times 10^5 [M_{\odot}], \end{aligned} \quad (19)$$

$$\begin{aligned} m_{ofs} &= \sum_{\Psi=540}^{780} \sigma(780) [M_{\odot}/\text{pc}^2] \times 1100 [\text{pc}^2] \\ &= 3.0 \times 10^5 [M_{\odot}], \end{aligned} \quad (20)$$

$$\begin{aligned} m_{out}v_{out} &= \sigma(780) [M_{\odot}/\text{pc}^2] \times V(780) [\text{pc}^2/\text{s}] \\ &= 2.7 \times 10^{-10} [M_{\odot}/\text{s}], \end{aligned} \quad (21)$$

$$\begin{aligned} m_{in}v_{in} &= \sigma(500) [M_{\odot}/\text{pc}^2] \times V(500) [\text{pc}^2/\text{s}] \\ &= 2.4 \times 10^{-10} [M_{\odot}/\text{s}], \end{aligned} \quad (22)$$

where the radial distance of the observed points from the galactic center is assumed to be about 3300 [pc] as given in [13]. The approximate value 150 [Myr] is in agreement with the expected range of 10 to 500 [Myr] estimated by the conventional theories [22].

5. Summary and discussion

In this paper, the CML for astronomical objects demonstrates that spiral arms are transient due to the "light-in and heavy-out" leading to the disappearance of traffic

jams. It was shown through the analysis of a spiral arm, in particular, from the following three aspects as traffic jams. First, the spiral arm is a type of traffic jam formed by jammed Keplerian gas around the central star. Second, the motion of the spiral arm is given as the movement of the traffic jam, which results from both a gas inflow into and outflow from the jam. Third, the disappearance of the traffic jam is caused by the gas flow rate difference between the light inflow and heavy outflow, which we have called the "light-in and heavy-out".

The "light-in and heavy-out" is also found in the gas observations of the spiral galaxy M51 [13]. The gas density and velocity changes are similar to those of the CML simulations.

According to the mechanism of the "light-in and heavy-out", we have proposed a general approximate formula for the lifetime of spiral arms. The approximate values obtained are in good agreement with the lifetimes in the CML simulations. Furthermore, we have estimated the lifetime of the spiral arm of M51 by using the proposed formula, and the approximate value is in agreement with the range expected by the conventional theories [22].

The proposed general approximate formula can be applied to various kinds of spiral arms. Indeed, we also estimate the lifetime of the spiral arm with a companion galaxy, which is just the other of the paired spiral arms in M51. The approximate value is larger than that of the spiral arm estimated in Section 4. The result is in agreement with the prediction of the conventional theories [22]. It may be due to the fact that the gas flow rate difference between the inflow and outflow becomes smaller due to the gravity of the companion. The details will be reported elsewhere.

There is another important unsettled issue, that is, the origin of spiral arms [7, 16]. We can show that the dynamic behavior of the central star should be the origin of spiral arms. It emerges from the gravitational interaction of the four massive gas clump components, which drives the nonlinear dynamics of the central star. The rich and diverse behavior including bifurcation, chaos and chaotic itinerancy [1, 23, 24] triggers gas ejection from the central star, and leads to the formation of spiral arms [14]. In astrophysics, the recent theoretical and observational studies of protoplanetary disks have highlighted the dynamics of the first core (such as the central star) induced by gravitational instability, towards the understanding of the formation mechanism of spiral arms. The highlights are: the fragmentation of the first core, outflows, bow shocks and gas clump ejections from the first core [25–27]. The relationship with these highlights will be reported in the next paper.

Acknowledgement

The author would like to thank T. Deguchi for critical reading and suggestive comments on the manuscript. The author also would like to thank K. Kaneko and I. Tsuda

for helpful discussions and warm encouragement. This work was supported by JSPS KAKENHI Grant Number JP20J12074.

Appendix A. Area-weighted average of field variables

We define the field variables at any position \mathbf{r} as the area-weighted average of the field variables on the lattice. The area-weighted average field variable $\tilde{a}^t(\mathbf{r})$ is given by the following equation with the field variables a_{ij}^t at the four nearest neighboring lattice points of the position \mathbf{r} :

$$\begin{aligned} \tilde{a}^t(\mathbf{r}) &= \tilde{a}^t(x, y) \\ &= \{1 - (x - [x])\} \{1 - (y - [y])\} a_{[x][y]}^t \\ &\quad + (x - [x]) \{1 - (y - [y])\} a_{[x]+1[y]}^t \\ &\quad + \{1 - (x - [x])\} (y - [y]) a_{[x][y]+1}^t \\ &\quad + (x - [x]) (y - [y]) a_{[x]+1[y]+1}^t, \end{aligned} \quad (\text{A.1})$$

where the coefficient of each field variable a_{ij}^t gives the area.

References

- [1] K. Kaneko and I. Tsuda, "Complex Systems: Chaos and Beyond", Springer-Verlag, Berlin, Heidelberg, New York (2001).
- [2] K. Kaneko ed., "Theory and Applications of Coupled Map Lattices", John Wiley & Sons, Chichester (1993).
- [3] T. Yanagita, "Coupled map lattice model for boiling", *Phys. Lett. A* **165** (1992) 405.
- [4] T. Yanagita and K. Kaneko, "Coupled map lattice model for convection", *Phys. Lett. A* **175** (1993) 415.
- [5] T. Yanagita and K. Kaneko, "Modeling and characterization of cloud dynamics", *Phys. Rev. Lett.* **78** (1997) 4297.
- [6] H. Nishimori and N. Ouchi, "Formation of ripple patterns and dunes by wind-blown sand", *Phys. Rev. Lett.* **71** (1993) 197.
- [7] J. Binney and S. Tremaine, "Galactic Dynamics", second edition, Princeton University Press, New Jersey (2008).
- [8] M. Tamura, "SEEDS—Strategic explorations of exoplanets and disks with the Subaru Telescope—", *Proc. Jpn. Acad., Ser. B* **92** (2016) 45.
- [9] C.C. Lin and F.H. Shu, "On the spiral structure of disk galaxies", *ApJ* **140** (1964) 646.
- [10] N. Kuno, T. Tosaki, N. Nakai and K. Nishiyama, "Two-arm spiral structure of molecular gas in the flocculent galaxy NGC 5055", *Publ. Astron. Soc. Japan* **49** (1997) 275.
- [11] M. Miyoshi, *et al.*, "Evidence for a black hole from high rotation velocities in a sub-parsec region of NGC4258", *Nature* **373** (1995) 127.
- [12] N.M. Murillo, S.P. Lai, S. Bruderer, D. Harsono and E.F. van Dishoeck, "A Keplerian disk around a Class 0 source: ALMA observations of VLA1623A", *A&A* **560** (2013) A103.
- [13] N. Kuno and N. Nakai, "Distribution and dynamics of molecular gas in the galaxy M51. III. Kinematics of molecular gas", *Publ. Astron. Soc. Japan* **49** (1997) 279.
- [14] E. Nozawa, "Coupled map lattice for the spiral pattern formation in astronomical objects", *Physica D* **405** (2020) 132377.
- [15] S.E. Meidt, R.J. Rand, M.R. Merrifield, R. Shetty and S.N. Vogel, "Radial dependence of the pattern speed of M51", *ApJ* **688** (2008) 224.
- [16] V. Christiaens, S. Casassus, S. Perez, G. van der Plas, and F. Ménard, "Spiral arms in the disk of HD 142527 from CO emission lines with ALMA", *ApJL* **785** (2014) L12.

- [17] W.W. Roberts Jr. and M.A. Hausman, "Spiral structure and star formation. I. Formation mechanisms and mean free paths", *ApJ* **277** (1984) 744.
- [18] A. Toomre, "On the gravitational stability of a disk of stars", *ApJ* **139** (1964) 1217.
- [19] K. Wada, J. Baba and T.R. Saitoh, "Interplay between stellar spirals and the interstellar medium in galactic disks", *ApJ* **735** (2011) 1.
- [20] R. Nishi, A. Tomoeda, K. Shimura and K. Nishinari, "Theory of jam-absorption driving", *Transp. Res. B* **50** (2013) 116.
- [21] V. Rana, *et al.*, "The broadband XMM-Newton and NuSTAR X-ray spectra of two ultraluminous X-ray sources in the galaxy IC 342", *ApJ* **799** (2015) 121.
- [22] F. Egusa, E.M. Cooper, J. Koda and J. Baba, "Gas and stellar spiral arms and their offsets in the grand-design spiral galaxy M51", *MNRAS* **465** (2017) 460.
- [23] K. Kaneko and I. Tsuda, "Chaotic itinerancy", *Chaos* **13** (2003) 926.
- [24] T. Tsuchiya, N. Gouda and T. Konishi, "Chaotic itinerancy and thermalization in a one-dimensional self-gravitating system", *Astrophys. Space Sci.* **257** (1997) 319.
- [25] T. Matsumoto and T. Hanawa, "Fragmentation of a molecular cloud core versus fragmentation of the massive protoplanetary disk in the main accretion phase", *ApJ* **595** (2003) 913.
- [26] E.I. Vorobyov, "Ejection of gaseous clumps from gravitationally unstable protostellar disks", *A&A* **590** (2016) A115.
- [27] A. Gusdorf, *et al.*, "Nature of shocks revealed by SOFIA OI observations in the Cepheus E protostellar outflow", *A&A* **602** (2017) A8.